Water Supply

IWA PUBLISHING

Water Supply Vol 24 No 9, 3015 doi: 10.2166/ws.2024.175

Hybrid intelligent and numerical methods to estimate the transmission coefficients of rectangular floating breakwaters

Hojat Karami[a,*] and Hasan Saghi[b]

[a] Department of Civil Engineering, Semnan University, Semnan, Iran
[b] Department of Civil Engineering, Hakim Sabzevri University, Sabzevar, Iran
*Corresponding author. E-mail: hkarami@semnan.ac.ir

ABSTRACT

Breakwaters are used to reduce incoming wave energy at harbors and shorelines. This paper presents a comparison of novel two-dimensional hybrid intelligent models for the idealization of the effects of waves on the performance of moored rectangular floating breakwaters (FBs). Fluid structure interactions (FSIs) were idealized by airy-type monochromatic regular waves generated in a numerical wave tank. The coupled Volume of Fluid-Fast Fictitious Domain (VOF-FFD) interpolation method was used to evaluate FB motions. Different forms of Least Squares Support Vector Machine Methods (LSSVMs) that utilized 183 data streams were used to model FB performance for different wave height-to-water depth ratios, dimensional aspect ratios, and specific length-to-water depth ratios. Of those, 80% were used to train the model and 20% to test it. Parametric studies have shown that during training a Least Squares Support Vector Machine Method-Bat Algorithm (LSSVM-BA) with $R^2 = 0.8725$, MAE = 0.0276, and RMSE = 0.0488 presents the most appropriate model for the evaluation of FB performance. Notwithstanding this, during testing a Least Squares Support Vector Machine Method-Cuckoo Search (LSSVM-CS) Algorithm with corresponding values of 0.6841, 0.0519, and 0.0708 performs better.

Key words: floating breakwaters (FBs), fluid structure interaction (FSI), hybrid intelligent models, least squares support vector machine (LSSVM)

HIGHLIGHTS

- Hybrid intelligent methods can effectively predict floating breakwater wave transmission coefficients.
- Novel two-dimensional hybrid models were used to model floating breakwater performance.
- LSSVM-BA and LSSVM-CS models performed best for training and testing, respectively.

GRAPHICAL ABSTRACT

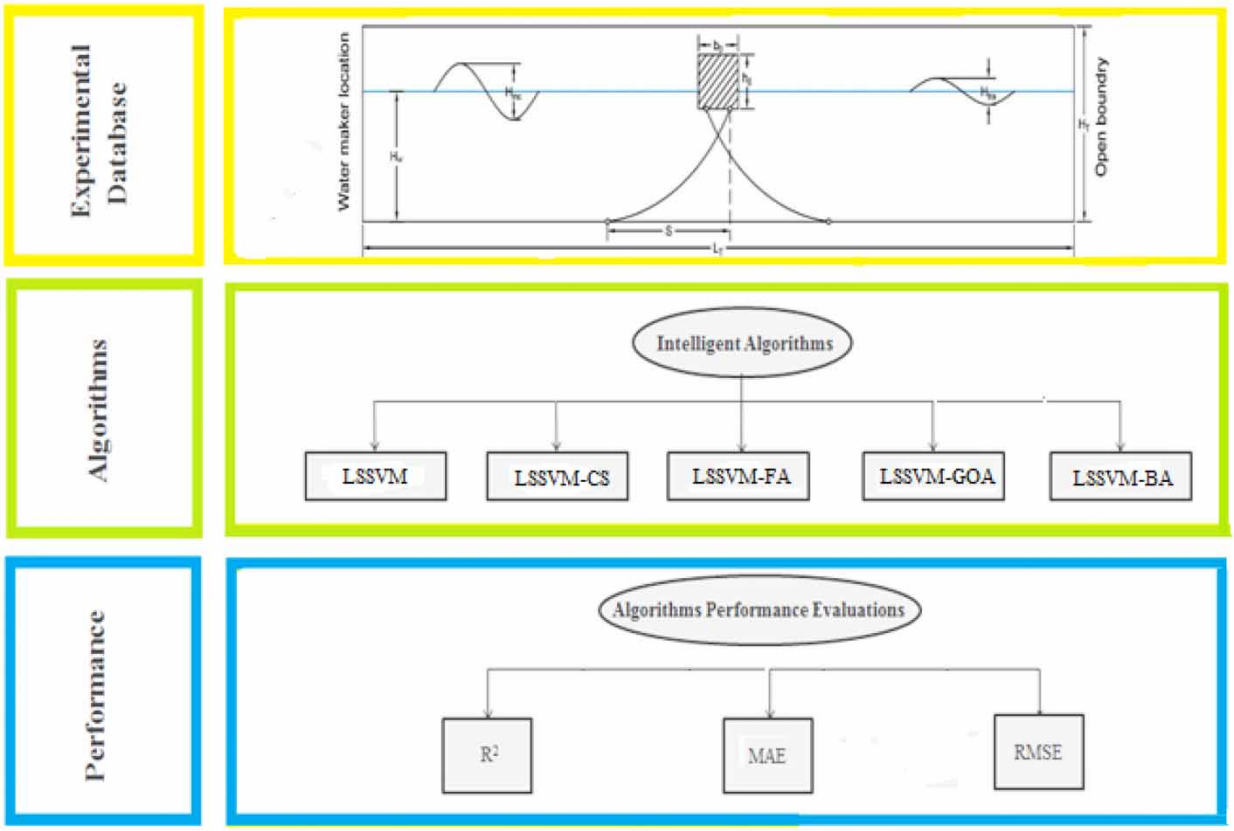

1. INTRODUCTION

Breakwaters are used to reduce incoming wave energy at harbors and shorelines. Contrary to mount breakwaters, floating breakwaters (FBs) are preferred as they are less costly in terms of installation and dissipate wave energy without constraining under-water flow in areas with tidal variations (Rafic & Pascal 2009; Dai *et al.* 2018; Ghazvinian & Karami 2024). The fast and accurate estimation of FB wave transmission coefficients remains challenging primarily because of the lack of unified models and associated uncertainties. Traditionally, methods using deterministic empirical methods and experimental results have been used (Ghazvinian *et al.* 2020a; Ghazvinian & Karami 2023a 2023b, 2023c). For example, Zhang & Li (2014) suggested the use of empirical formulae based on modified Boussinesq wave equations for the fast evaluation of wave transmission coefficient on permeable rubble mounds and pile-type breakwaters. van der Meer & Daemen (1994) developed practical design formulas and graphs, based on extensive experimental data, to predict the transmission wave for statically stable submerged, low-crested, and dynamically stable FB. d'Angremond *et al.* (1996) introduced an expression for the transmission coefficient of a low-crested breakwater based on structural and wave parameters. Detailed laboratory tests to estimate transmission coefficients have also been carried out by Kramer *et al.* (2005), Calabrese *et al.* (2008), Peng *et al.* (2009), Hur *et al.* (2012), Melito & Melby (2002), and Laju *et al.* (2011). From an overall perspective comparisons of laboratory tests against empirical formulae show that the results of van der Meer & Daemen (1994) can be applied to rubble mound breakwater installations. On the other hand, when the equation by d'Angremond *et al.* (1996) is used, large deviations may occur in the case of permeable breakwaters with large transmission coefficients.

The hydrodynamic efficiency of FB may vary depending on their design specification and operational conditions. For example, Ji *et al.* (2015, 2016, 2017) compared linear hydrodynamic theory and experiments to show that a cylindrical FB (CFB) consisting of rigid cylinders and a flexible mesh cage has better hydrodynamic performance than double pontoon-type structures. Liu & Wang (2020) investigated the hydrodynamics of moored box-type FB with different cross-sections using the smoothed particle hydrodynamics (SPH) method. Their study accounted for key hydrodynamic parameters such

as the breakwater density, immersion depth, ballast-water gravity and wave conditions and showed that FB performance may be significantly affected by the wave conditions and immersion depth. Ji *et al.* (2018) studied experimentally the hydrodynamic performance of double-row rectangular FB with porous plates. They carried out a series of two-dimensional experiments and concluded that double-row FB systems perform better to mitigate the transmission wave. Cho (2016) studied the influence of wave transmission on an innovative floating rectangular breakwater. Their results showed that unique design characteristics such as porosity and deep side plates may reduce the influence of hydrodynamic loads.

Intelligent and hybrid methods are computationally versatile and therefore useful for the evaluation of the hydrodynamic performance of an FB. Basser *et al.* (2014) compared the application of two support vector regression (SVR) FB types, namely polynomial-based (SVR_poly) and radial basis function (RBF)-based SVR (SVR_rbf) with adaptive neuro fuzzy system (ANFIS), and adaptive neural network (ANN) to estimate the best parameters for the design of a protective spur dike. The authors observed that the SVR achieves better accuracy in terms of percentage reduction in the scour depth with a smaller network size, compared to the ANFIS and ANN approaches. Also, the SVR_rbf model having values of 0.7200 and 0.1200, respectively, for R and RMSE (root mean square error) indicators is more accurate compared to the SVR_poly approach with $R = 0.6210$ and $\mathrm{RMSE} = 0.1500$.

More recently, the work by Ehteram *et al.* (2018) demonstrated that genetic, particle swarm and especially shark algorithms can be efficient for optimization in reservoir operation and water supply. However, the complexity of such methods implies the need for further testing and validation. As an alternative Saghi *et al.* (2021) introduced a fast and efficient numerical model for the idealization of moored FB motions in regular and irregular waves. In their work, they assessed the hydrodynamic performance of an FB by the Cuckoo Search-Least Square Support Vector Machine model (CS-LSSVM) and demonstrated that a suitable combination of sidewall mooring angle and the aspect ratio of the FB could help attenuate incoming waves to a minimum height.

The review of previous studies shows that so far, few researches have been done in the field of using intelligent methods to idealize the effects of waves on the performance of moored rectangular FBs. This paper presents a rapid method for the prediction of the transmission coefficient of a rectangular FB. The numerical model of Saghi *et al.* (2021) which combines a fast fictitious domain with a volume of fluid (VOF) method to track free surface effects is used for motion prediction. A brief description of different hybrid intelligence models that were assessed and compared in this study is given in Section 2 alongside an explanation of the methods and statistical tools used to evaluate the various predictions. The results presented in Section 3 discuss the performance indicators through a comprehensive set of performance diagrams. Conclusions are given in Section 4.

2. MATERIALS AND METHODS

2.1. Governing equations and boundary conditions

The numerical model used to generate airy waves and simulate the FB motions is shown in Figure 1.

In this figure, a moored floating breakwater with dimensions b_0 and h_0 is placed in a part of the wave tank such that the incoming wave height is equal to H_{inc} and the transmitted wave height is equal to H_{tra}.

The fluid was considered viscous and incompressible. Accordingly, the governing equations were defined as per (Saghi & Lakzian 2017):

$$\nabla.V = \frac{\partial u}{\partial x} + \frac{\partial v}{\partial y} = 0 \tag{1}$$

$$\frac{\partial V}{\partial t} + (V.\nabla)V = \frac{-\nabla p}{\rho} + g + \nabla.((\upsilon + \upsilon_t)(\nabla V + \nabla V^T)) \tag{2}$$

where V is the velocity vector, u and v are the velocity components in the x and y directions, respectively, t is the time, p is the dynamic pressure, g is the gravitational acceleration, ∇ is the gradient operator, υ is the kinematic viscosity, and υ_t is the turbulent viscosity.

These equations were solved by using the SMAC method (Saghi 2018). The k–ε model was also used to idealize the effects of turbulence (Shen *et al.* 2004; Saghi & Lakzian 2019). At the bottom of the domain, zero normal velocity and horizontal no-slip conditions were implemented. At the cell boundary, where the computational cell is adjacent to the solid cell, a no-slip

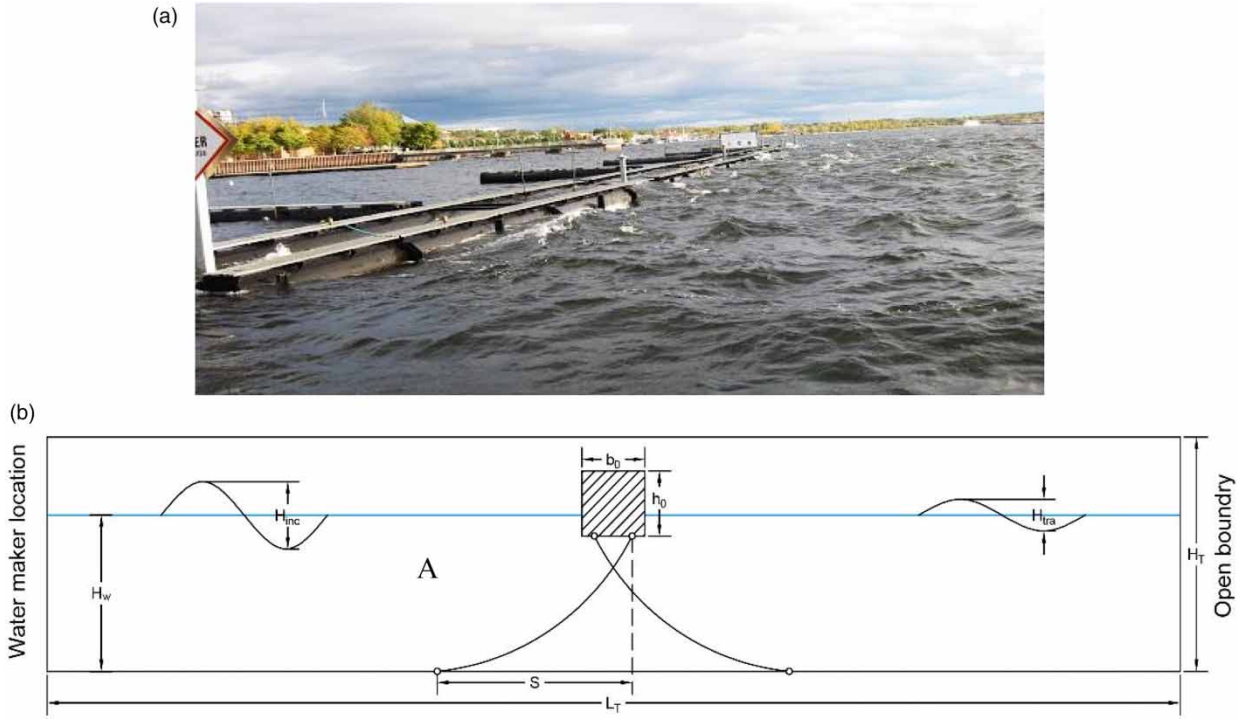

Figure 1 | (a) A real FB (Marine biotech, 2007) and (b) schematic sketch of NWT rectangular moored FB configuration.

wall boundary condition was used to idealize the velocity component. At the outflow boundary, the open boundary condition was used to eliminate the propagation of the reflected waves from the boundary into the domain (Saghi *et al.* 2012). In the inflow boundary, the velocity was calculated with a piston type wave maker at each time step. The Youngs VOF method is used for free surface tracking (Youngs 1982). Thus, the interface within the cells was approximated by straight lines of different orientations. To generate an airy wave, the velocity conditions in the input boundary (i.e., in way of the wave maker location) were based on linear theory (Liu & Li 2013). Coupling of VOF-FFD methods was used to model the FB motions (Mirzaii & Passandideh-Fard 2012). The wave transmission coefficient was defined as:

$$K_t = \frac{H_{\text{tra}}}{H_{\text{inc}}} \tag{3}$$

where H_{inc} and H_{tra} are the incident and transmitted wave heights, respectively. The average transmitted wave height after the initial transient (H_{tra}) was used to calculate K_t as:

$$K_t = f\left(\frac{H_{\text{inc}}}{Hw}, AR, \frac{\sqrt{A_b}}{H_w}\right) \tag{4}$$

where $\text{AR} = b_0/h_0$, $A_{\text{b}} = b_0 h_0$, and b_0 and h_0 are the breakwater dimensions in the x and y directions, respectively (see Figure 1).

2.2. Model validation

An airy wave of 1 cm amplitude and 1.2 s period was generated in the NWT for different mesh sizes. Results showed a mesh size independence for $d_x = 0.02$ m and $d_y = 0.01$ m. Dynamic time steps that satisfy the CFL number of 0.3 were also used (Nichols *et al.* 1980). The wavemaker theory was used to validate the model, and the results are shown in Figure 2. The prediction of the wave transmission has been validated against the experimental results of Cui *et al.* (2020) and the results are shown in Figure 3. It can be seen as a good agreement between the results.

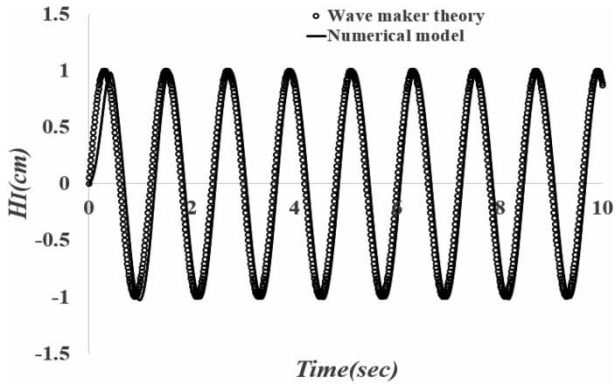

Figure 2 | Model validation in the generation of the airy wave by using a wave maker theory.

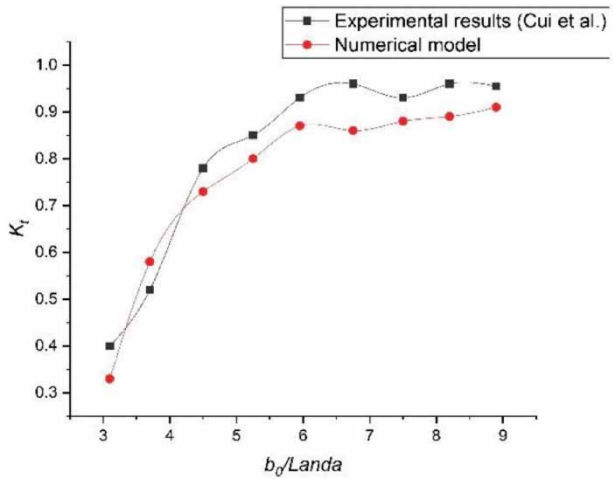

Figure 3 | Comparison of transmission coefficients estimated by the developed model and the experimental results of Cui *et al.* (2020).

2.3. Intelligent hybrid models

An LSSVM model (Ghazvinian *et al.* 2020b, 2021) was used to estimate the transmission coefficient of the rectangular floating breakwater. Various optimization algorithms namely the Bat Algorithm (BA), Firefly Algorithm (FA), Grasshopper Optimization Algorithm (GOA), and Cuckoo Search (CS) Algorithm were coupled to the LSSVM model to find the optimum parameters of the model. Input parameters comprised 183 big data streams including H_I/H_w (the ratio of incident wave height-to-water depth), AR (breakwater aspect ratio), and $A_b^{0.5}/H_w$ (the ratio of the specific length of the breakwater to water depth) in different conditions. The number of input data streams in the training mode of the four proposed models was 146. This corresponds to 80% of the overall data streams made available. The remaining testing module comprised 37 data streams.

2.3.1. LSSVM model

LSSVMs are sets of related supervised learning methods used for classification and regression analysis. In such methods, the non-linear relationship between inputs and outputs is converted to a linear relationship by mapping inputs from a space with lower dimensions to a space with higher dimensions (Suykens 2001; Anandhi *et al.* 2008) as follows (see Figure 4):

$$y' = \sum_{i=1}^{3} w_i K(I, I_i) + b \tag{5}$$

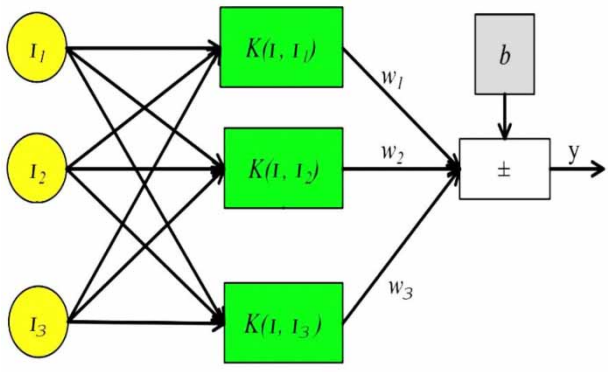

Figure 4 | The structure of the LSSVM model to predict transmission coefficient of a FB.

The risk bound was minimized by the function:

$$Min{:}\psi(W, e) = \frac{1}{2}WW^T + \frac{1}{2}C\sum_{i=1}^{N} e_i \tag{6}$$

$$e_i = y_i - y'_i \tag{7}$$

Based on Figure 4, the input and output parameters are defined as, $[I_1, I_2, I_3] = \left[H_I/H_w, AR, \sqrt{A_b}/H_w\right]$ and, $y = k_t$, respectively.

2.3.2. Optimization algorithms

The BA is a new meta-innovative algorithm inspired by bat positioning behavior (Cheng 2010). This algorithm is based on the echolocation which is a sonar wave emitted by the microbats. It helps bats find prey and discriminate against the different kinds of obstacles or dangers on their way toward the prey in complete darkness (Srivastava & Sahana 2019).

A BA comprises the following three basic steps:

1. All bats can make a sound and receive it. Based on this ability, they can distinguish between food sources and barriers.
2. Bats fly randomly and while flying they have wavelength (λ), constant frequency ($f_{\min}$) and velocity (V_i) in the X_i position. They can also generate sound pulses between 0 and 1.
3. The loudness of bats can vary from a large positive A_0 value to a small positive $A_{\min}$ value.

It can be assumed that the value of frequency (f) can vary between $f_{\min}$ and $f_{\max}$ and the corresponding wavelength between $\lambda_{\min}$ and $\lambda_{\max}$. Wavelength amplitude can also vary. The wavelength should be selected based on the problem search space. X_{best} in the BA is considered the universal answer to the problem or the best position of the bats. Equations (8)–(10) show the updated frequency, speed, and position of bats, respectively.

$$f_i = f_{\min} + (f_{\max} - f_{\min})\beta \tag{8}$$

$$v_i^t = v_i^{t-1} + (x_i^{t-1} - x_{\text{best}})f_i \tag{9}$$

$$x_i^t = x_i^{t-1} + v_i^t \tag{10}$$

where f_i represents the frequency bat i, v_i^t is the new speed of bat, v_i^{t-1} is the previous speed, x_i^t the new position, x_i^{t-1} the previous position and β is a random vector with arrays between 0 and 1. In the first step, a random number between $f_{\min}$ and $f_{\max}$ is assigned to each bat. The bat speed and position are then updated based on Equations (9) and (10). Then a random number is generated. If the pulse generation rate is less than this random number, the local search is performed using the production of a random step based on Equation (11):

$$x_i^t = x_i^{t-1} + \varepsilon A^t \tag{11}$$

where ε is a random number and A^t is the average volume (Farzin *et al.* 2018).

The FA is a population-based and random optimization algorithm based on the behavior of fireflies in placental uptake as introduced by Yang (2009). The three basic hypotheses of this algorithm are:

(1) There is no specific gender for fireflies.
(2) Each firefly is absorbed by other fireflies according to their light intensity.
(3) In problems of maximization, the amount of light intensity is directly related to the objective function, and in problems of minimization, the intensity of light is inversely related to the objective function.
(4) The movement of a firefly to another firefly is defined as:

$$x_i^{t+1} = x_i^t + \beta_0 e - \gamma r_{ij}^2 (x_j^t - x_i^t) + \alpha(rand - 0.5) \tag{12}$$

The Grasshopper Algorithm (GA) simulates the swarming behavior of grasshoppers in nature. The mathematical equations and formulas proposed for this algorithm are given in Saremi *et al.* (2017). In this algorithm, the position of the grasshoppers in the swarm represents a possible solution to a given optimization problem. The position of the *i*th grasshopper is denoted as X_i is:

$$X_i = S_i + G_i + A_i \tag{13}$$

where S_i, G_i, and A_i interact with the effect of social, gravity, and wind on the movement of grasshopper, respectively.

The CS algorithm is based on the cuckoo's deceptive behavior when laying its eggs in other birds' nests (Yang & Deb 2009). In general, this algorithm has three general rules:

(1) Each cuckoo lays an egg only once at a time and lays it in a randomly selected nest.
(2) The best nests and the highest quality eggs are passed on to the next generation.
(3) The number of host nests available is constant and cuckoo eggs will be identified by the host bird of probability P_a

Each of these selected algorithms has its own advantages. For example, the advantage of the BOA is the powerful combination between a population-based algorithm and the local search, however, it is more efficient for local searches (Heraguemi *et al.* 2015). On the other hand, an advantage of CS is that its global search uses L'evy flights or processes, rather than standard random walks. As L'evy flights have infinite mean and variance, CS can explore the search space more efficiently than algorithms by standard Gaussian processes. This advantage, combined with both local and search capabilities and guaranteed global convergence, makes CS very efficient (Yang & Deb 2014). The GA allows for the participation of all search agents. The algorithm avoids falling into the trap of local optimization and then convergence and creating a balance between global and local search capabilities (Saremi *et al.* 2017). Finally, the advantage of the firefly optimization algorithm is that it automatically subdivides data streams and can deal with multimodality (Yang & He 2013).

2.3.3. Coupling of LSSVM and optimization algorithms

A coupling of different optimization algorithms and LSSVM was used to evaluate the performance of a rectangular FB. The key steps of the coupling process are summarized below and demonstrated in Figure 5.

(1) Determine the basic parameters of optimization algorithms.
(2) Divide laboratory data into two courses of training and testing.
(3) Produce the primary population.
(4) Effect min. square backup vector machine training according to training course data and the decision variables of the optimization algorithm.
(5) Test the least squares backup vector machine and determine the objective function for the optimization algorithm.
(6) Terminate the condition control and if it is observed, return the optimal values of the parameters of the least squares support vector machine. If this is not possible then update the position in the optimization algorithms and go back to step 4.

2.4. Statistical indicators

In this research, statistical indicators including the coefficient of determination (R^2) (Samii *et al.* 2023), mean average error (MAE) (Karami & Ghazvinian 2022), and RMSE (Karami *et al.* 2023) were defined to determine the accuracy of the

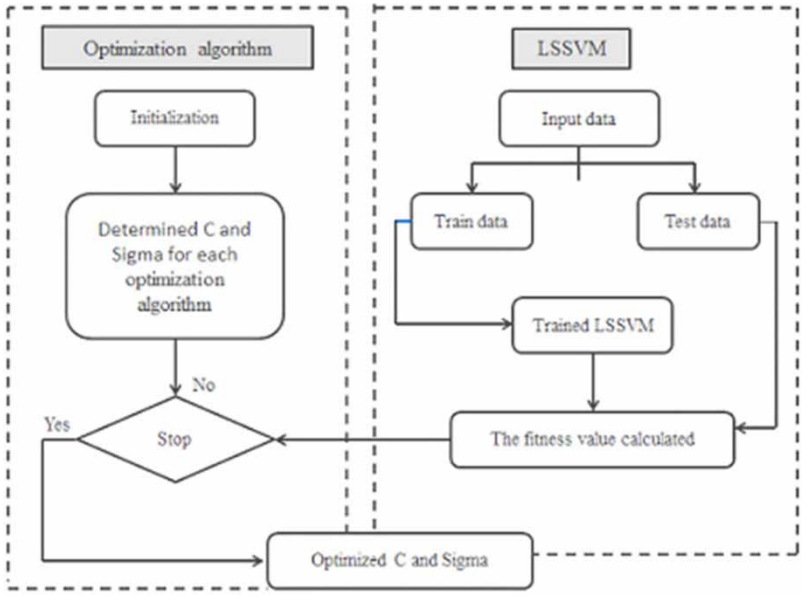

Figure 5 | Flow chart of couple of LSSVM and optimization algorithms.

intelligent models, as follows:

$$R^2 = 1 - \left[\frac{\sum_{i=1}^{N} (O - P)^2}{\sum_{i=1}^{N} O^2 - \left(\sum_{i=1}^{N} P^2 / N \right)} \right] \tag{14}$$

$$\text{MAE} = \frac{1}{N} \sum_{i=1}^{N} |O - P| \tag{15}$$

$$\text{RMSE} = \sqrt{\frac{\sum_{i=1}^{N} (O - P)^2}{N}} \tag{16}$$

R^2 indicates the proportion of the variance between the observed values and the predicted values from intelligent models. The closer it is to 1, the better the correlation between the observed data and the results of the intelligent model. The MAE and RMSE indices help identify the error band. The closer the value of these indices is to zero, the more accurate the answer

Table 1 | The results of evaluation indicators for different intelligent models

Model number	Statistical parameter / Model name	R^2		MAE		RMSE	
		train	test	train	test	train	test
1	LSSVM	0.1061	0.1962	0.0926	0.0910	0.1111	0.1120
2	LSSVM-CS	0.7847	0.6841	0.0374	0.0519	0.0546	0.0708
3	LSSVM-FA	0.7849	0.6781	0.0365	0.0365	0.0714	0.0714
4	LSSVM-GOA	0.7848	0.6674	0.0361	0.0361	0.0727	0.0727
5	LSSVM-BA	0.8275	0.5989	0.0276	0.0276	0.0778	0.0778

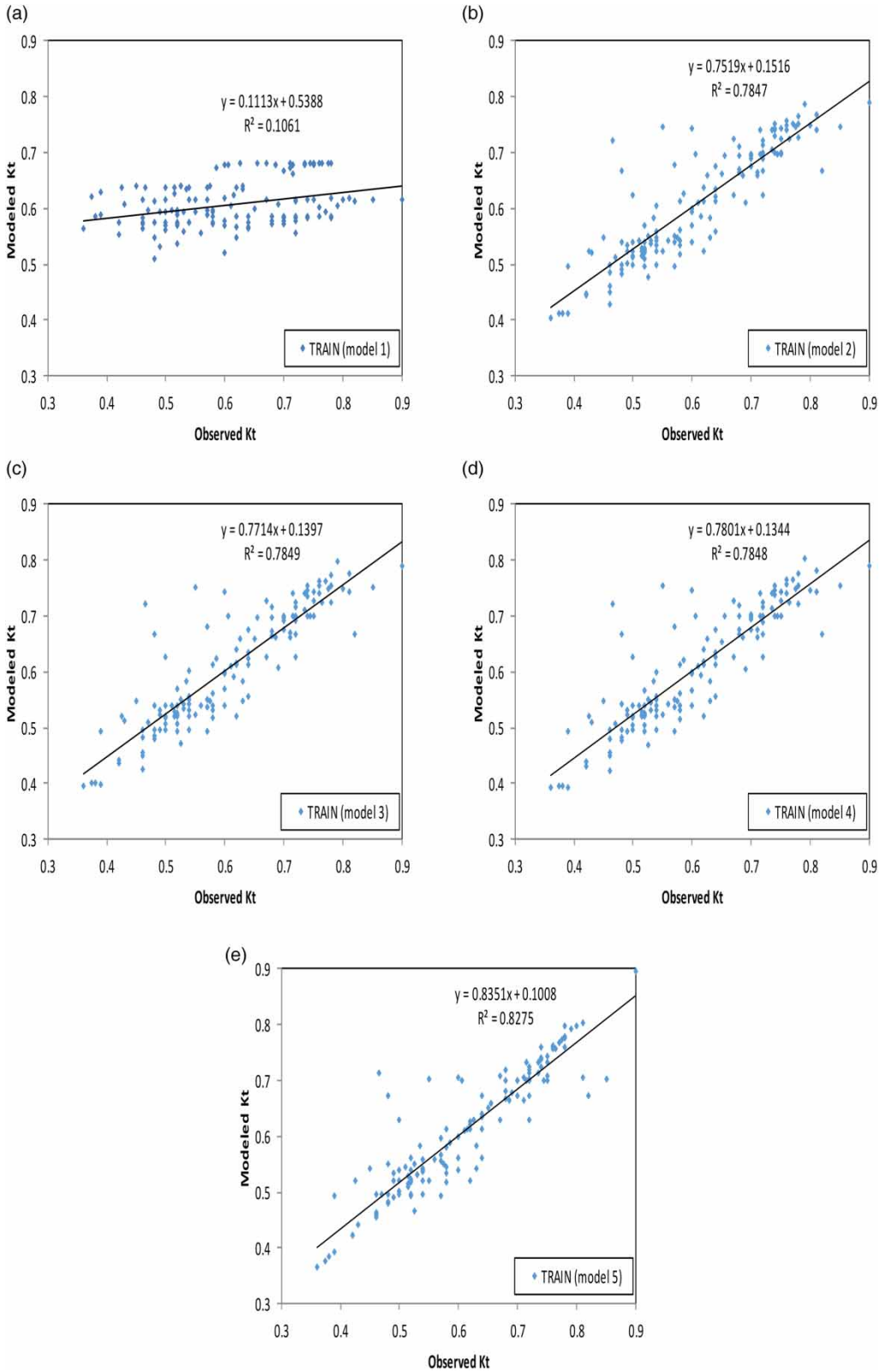

Figure 6 | The estimated transmission coefficient of the models relative to the observed one (estimated using the developed model) in the training step: (a) model 1, (b) model 2, (c) model 3, (d) model 4, and (e) model 5.

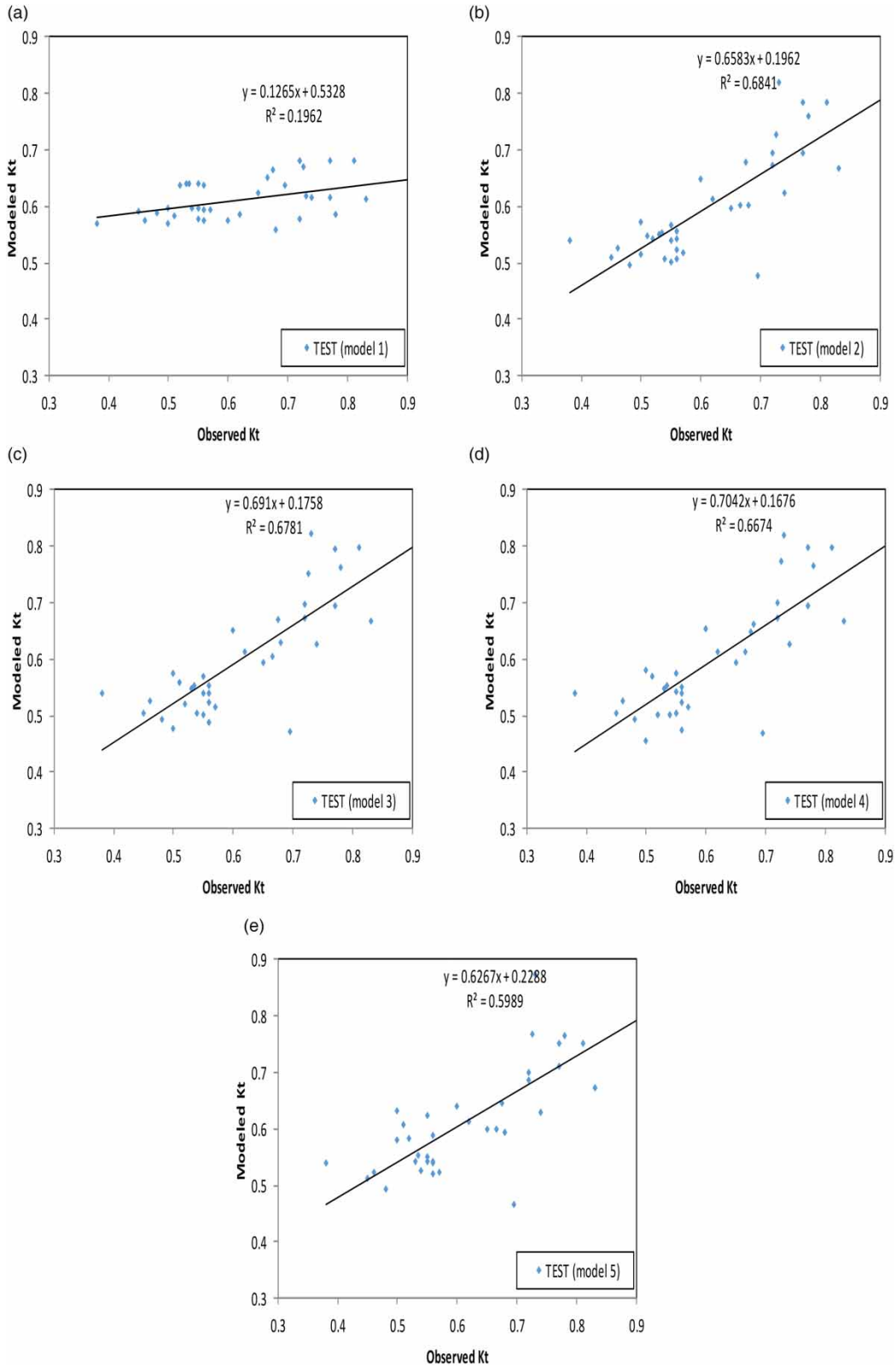

Figure 7 | The estimated transmission coefficient of the models relative to the observed one (estimated by using the developed model) in the testing step: (a) model 1, (b) model 2, (c) model 3, (d) model 4, and (e) model 5.

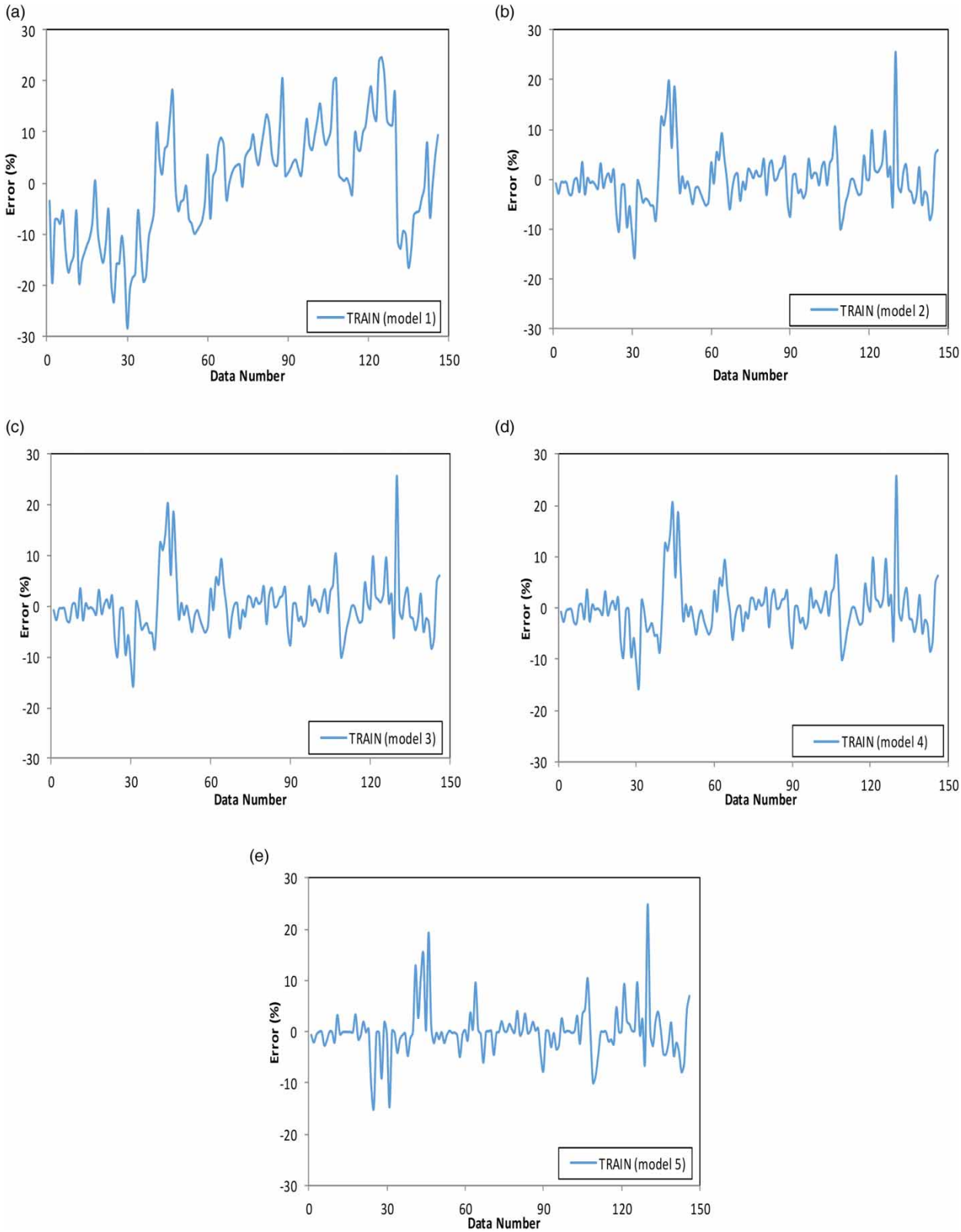

Figure 8 | The prediction error distribution of the models in the training step: (a) model 1, (b) model 2, (c) model 3, (d) model 4, and (e) model 5.

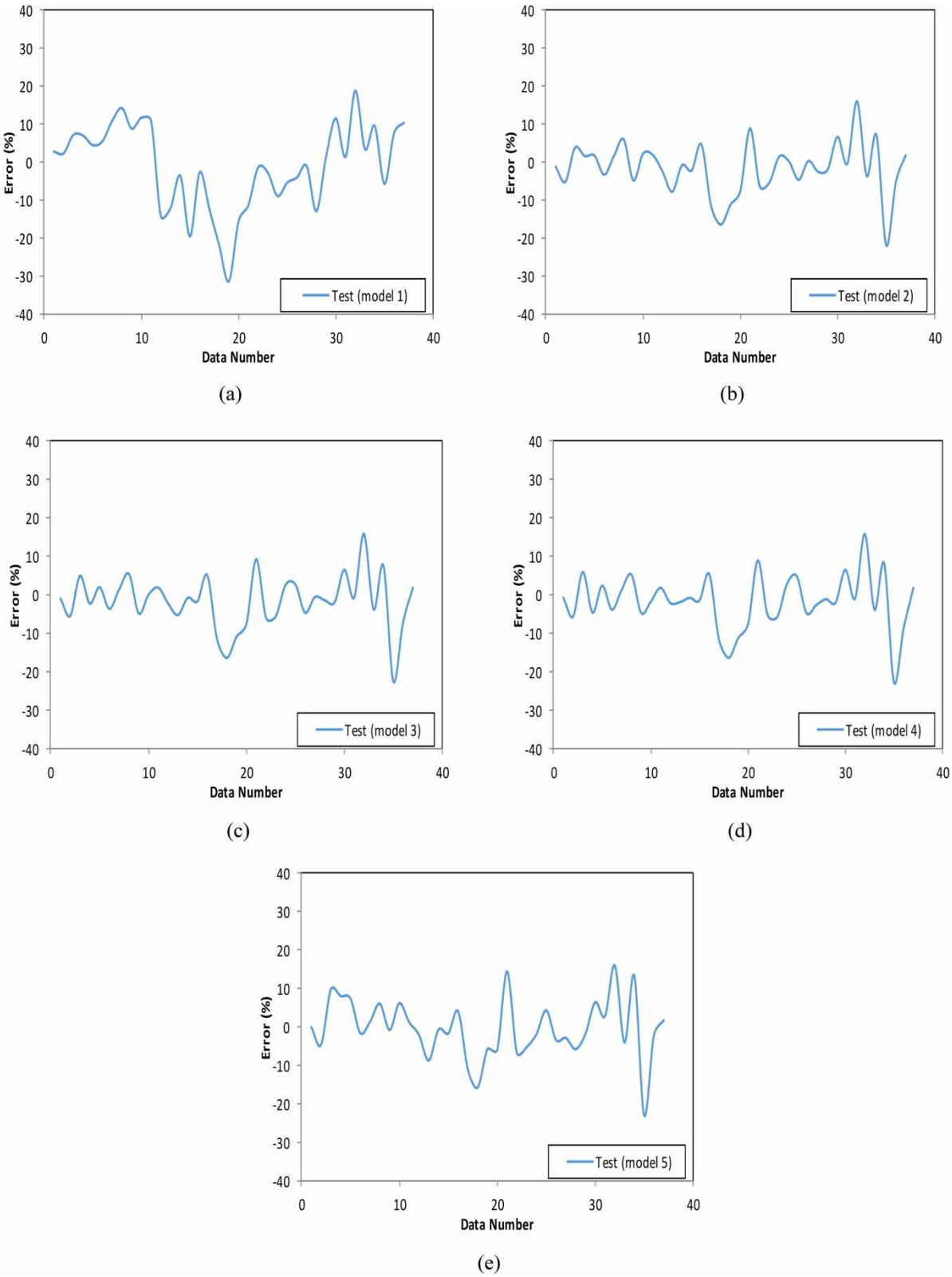

Figure 9 | The prediction error distribution of the models in the testing step: (a) model 1, (b) model 2, (c) model 3, (d) model 4, and (e) model 5.

predicted by the smart model (Dadrasajirlou *et al.* 2022). In Equations (14)–(16), term O represents the value obtained from the numerical model, P is the value predicted using the intelligent model, and N is the number of variables.

3. RESULTS AND DISCUSSION

Table 1 presents the results of evaluation indicators for five different models in training and test courses. The models compared were LSSVM (model 1), LSSVM-CS (model 2), LSSVM-FA (model 3), LSSVM-GOA (model 4), and LSSVM-BA (model 5). Results show that in the training course, model 5 with $R^2 = 0.8275$ is superior to all other models. In this training period, Model 5 with MAE = 0.0276 and RMSE = 0.0488 is better performing. However, the value of the determination coefficient in model 2 (R^2≦0.6841) is higher than intelligent all other models. Thus, this model is more accurate. Within the testing period indices MAE and RMSE for model 2 are 0.0519 and 0.0708 and, therefore, lower than all other models. Thus, model 2 has the highest predictive power.

Figure 6 compares K_t throughout the training course for both observed and predicted models 1–5. The results show that model 5 has the highest correlation and density. Consequently, models 3, 4, 2, and 1 with correlation values 0.7849, 0.7848, 0.7847, and 0.1061, respectively, follow the ranks.

Figure 7 shows the correlation of laboratory data and all intelligent models during the test period. Model 2 with a correlation coefficient of 0.6841 has better performance. Models 3, 4, 5, and 1 follow, respectively, this value.

The K_t prediction error distribution of all models in both the training and testing phases are summarized in Figures 8 and 9, respectively. In the training phase, the error range of Models 5 and 1 are (−15 to 25%) and (−29 and 25%), respectively. However, Models 4, 3 and 2 consistently present errors between −16 and 26%. In the testing phase, the error range of model 5 is between −23 and 17%. The error range of models 4,3 and 2 are between −23 and 16%. However, model 1 error is between −32 and 19%.

Previously, in the research of Hu *et al.* (2021), better performance of intelligent models was seen in the training course than in the test course.

From an overall perspective, the results shown in Figure 10 show that model 2 corresponding to LSSVM-CS presented originally by Saghi *et al.* (2021) has the minimum prediction error distribution. So, this model was chosen as the best hybrid intelligent model to predict the transmission coefficient of the rectangular FB considered. In turn, to evaluate the efficiency of model 2, the transmission coefficient was estimated for the cases summarized in Table 2. Since the numerical error varies between (2 and 10)% this comparison re-affirms the acceptable accuracy of the model.

In the Taylor diagram (Taylor 2001) shown in Figure 10, the longitudinal distance from the origin of the coordinates represents the standard deviation, the radial lines represent the correlation coefficient, and the segmental lines represent the root

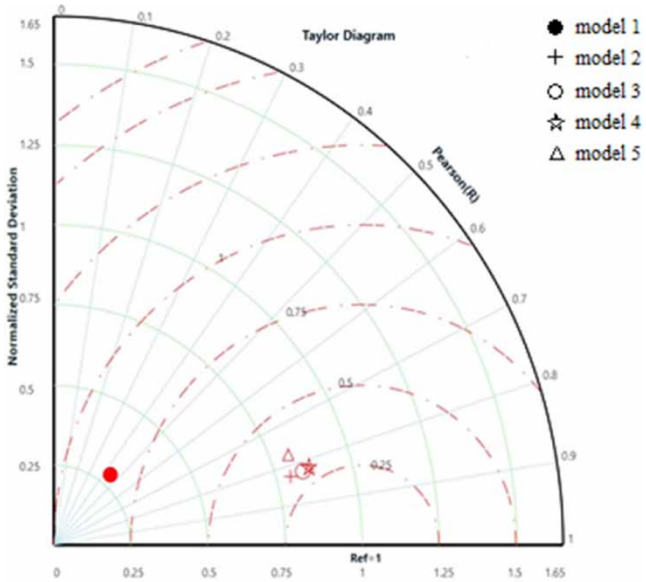

Figure 10 | Taylor diagrams of estimated values in the testing phase.

Table 2 | Estimation of transmission coefficient of rectangular FBs with different AR and its error by using model 2

Sample number	H_l/H_w	AR	$\sqrt{A_b}/H_w$	K_t (EXP.)	K_t (model 2)	Relative error
1	0.067	2.560	0.416	0.55	0.5388	−0.0203
2	0.033	2.250	0.500	0.50	0.5162	0.0324
3	0.033	4.000	0.417	0.48	0.4963	0.0339
4	0.025	3.240	0.625	0.72	0.6955	−0.0340
5	0.025	1.440	0.624	0.68	0.6025	−0.1139
6	0.025	1.000	0.625	0.62	0.6120	−0.0129
7	0.025	1.960	0.626	0.78	0.7585	−0.0275
8	0.025	4.710	0.749	0.60	0.6468	0.0780

mean square error values. By increasing the circle segment, the mentioned parameter value is increased. This means that during the testing phase models 2 and 1 have the highest and lowest accuracy, respectively.

4. CONCLUSIONS

This paper presented a comparison of novel two-dimensional hybrid intelligent models for the idealization of the effects of waves on the performance of moored rectangular FB. FSI modeling assumed airy and irregular waves generated in a numerical wave tank and a coupled VOF-FFD method was used to evaluate motions. From an overall perspective, results show that hybrid intelligent methods can be fast and practical in terms of predicting the values of FB wave transmission coefficients. A comparison of K_t for five hybrid intelligent models showed that model 5 (LSSVM-BA) performed the best with training error between −15 and 25%. However, during testing model 2 (LSSVM-CS) appeared to present a more appropriate error band in the range of −22 and 16%. It may therefore be concluded that whereas the training period can be used for preliminary algorithm evaluation, the most suitable phase to choose the best algorithm for FB performance optimization could be the test period. This is because new data are used during the test period and, therefore, the accuracy of each algorithm is determined at this stage.

4.1. Future works

The simultaneous use of intelligent and numerical methods can be very useful and efficient in increasing both the accuracy and the ability to quickly predict various hydrodynamic parameters. Therefore, this technique can be applied to the simulation of various marine structures, including other types of breakwaters.

FUNDING

This research did not receive any specific grant from funding agencies in the public, commercial, or not-for-profit sectors.

DATA AVAILABILITY STATEMENT

All relevant data are included in the paper or its Supplementary Information.

CONFLICT OF INTEREST

The authors declare there is no conflict.

REFERENCES

Anandhi, A., Srinivas, V. V., Nanjundiah, R. S. & Kumar, D. N. 2008 Downscaling precipitation to river basin in India for IPCC SRES scenarios using support vector machine. *International Journal of Climatology* **28** (3), 401–420.

Basser, H., Karami, H., Shamshirband, S., Jahangirzadeh, A., Akib, S. & Saboohi, H. 2014 Predicting optimum parameters of a protective spur dike using soft computing methodologies–A comparative study. *Computers & Fluids* **97**, 168–176.

Calabrese, M., Buccino, M. & Pasanisi, F. 2008 Wave breaking macro features on a submerged rubble mound breakwater. *Journal of Hydro-Environment Research* **1** (3–4), 216–225. doi:10.1016/10.1016/j.jher.2007.11.003.

Cheng, L. I. 2010 A new metaheuristic bat-inspired algorithm. *Computer Knowledge. Technology* **284**, 65–74.

Cho, I. H. 2016 Transmission coefficients of a floating rectangular breakwater with porous side plates. *International Journal of Naval Architecture and Ocean Engineering* **8**, 53–65.

Cui, J., Liu, H., Deng, X., Tao, S. & Li, Q. 2020 An experimental study on hydrodynamic performance of a box-floating breakwater in different terrains. *Journal of Marine Science and Technology* **25**, 991–1009. doi:10.1007/s00773-019-00695-4.

Dadrasajirlou, Y., Ghazvinian, H., Heddam, S. & Ganji, M. 2022 Reference evapotranspiration estimation using ANN, LSSVM, and M5 tree models (Case study: Of babolsar and Ramsar Regions, Iran). *Journal of Soft Computing in Civil Engineering* 6 (3), 103–121. http://www.jsoftcivil.com/article_158359.html.

Dai, J., Wang, C. M., Utsunomiya, T. & Duan, W. 2018 Review of recent research and developments on floating breakwaters. *Ocean Engineering* **158**, 132–151.

D'Angremond, K., van der Meer, J. W. & de Jong, R. J. 1996 Wave transmission at low crested structures. In: *Proceedings of the 25th International Conference on Coastal Engineering*. ASCE, Florida, USA, pp. 2418–2427.

Ehteram, M., Karami, H., Mousavi, S. F., Farzin, S. & Kisi, O. 2018 Evaluation of contemporary evolutionary algorithms for optimization in reservoir operation and water supply. *Journal of Water Supply: Research and Technology* **67**, 54–67.

Farzin, S., Karami, H., Valikhan Anaraki, M. & Ehteram, M. 2018 The application of bat algorithm for economical design of open channels. *Iranian Journal of Irrigation & Drainage* **12** (3), 635–646.

Ghazvinian, H. & Karami, H. 2023a Laboratory comparison of vegetation and gravel on parameters affecting urban floods under different rainfall and runoff conditions. *Journal of Water and Climate Change* **14** (12), 4763–4781.

Ghazvinian, H. & Karami, H. 2023b Laboratory study of the effect of vegetation and gravel on runoff parameters under variable rainfall intensities. *Water Science & Technology* **88** (9), 2423–2442.

Ghazvinian, H. & Karami, H. 2023c Effect of rainfall intensity and slope at the beginning of sandy loam soil runoff using rain simulator (Case study: Semnan city). *Journal of Water and Soil Science* **26** (4), 319–334. http://jstnar.iut.ac.ir/article-1-4274-en.html.

Ghazvinian, H. & Karami, H. 2024 Evaluating the effect of geocell with vegetation and gravel on changes in the effective parameters of runoff using a rainfall simulator (case study: Iran). *Physics and Chemistry of the Earth, Parts A/B/C* **134**, 103585.

Ghazvinian, H., Farzin, S., Karami, H. & Mousavi, S. F. 2020a Investigating the effect of using polystyrene sheets on evaporation reduction from water-storage reservoirs in arid and semiarid regions (Case study: Semnan city). *Journal of Water and Sustainable Development* **7** (2), 45–52. https://jwsd.um.ac.ir/article_32593.html.

Ghazvinian, H., Karami, H., Farzin, S. & Mousavi, S. F. 2020b Experimental study of evaporation reduction using polystyrene coating, wood and wax and its estimation by intelligent algorithms. *Irrigation and Water Engineering* **11** (2), 147–165. http://www.waterjournal.ir/article_120727.html.

Ghazvinian, H., Karami, H., Farzin, S. & Mousavi, S.-F. 2021 Introducing affordable and accessible physical covers to reduce evaporation from agricultural water reservoirs and pools (field study, statistics, and intelligent methods). *Arabian Journal of Geosciences* **14** (23), 2543. https://link.springer.com/10.1007/s12517-021-08735-3.

Heraguemi, K. E., Kamel, N. & Drias, H. 2015 Multi-population cooperative bat algorithm for association rule mining. In: *Computational Collective Intelligence. 7th International Conference, ICCCI 2015, Madrid, Spain, September 21–23, 2015, Proceedings, Part I*. Springer International Publishing, Cham, Switzerland, pp. 265–274.

Hu, Z., Karami, H., Rezaei, A., DadrasAjirlou, Y., Piran, M. J., Band, S. S. & … Mosavi, A. 2021 Using soft computing and machine learning algorithms to predict the discharge coefficient of curved labyrinth overflows. *Engineering Applications of Computational Fluid Mechanics* **15** (1), 1002–1015.

Hur, D. S., Lee, W. D. & Cho, W. C. 2012 Characteristics of wave run-up height on a sandy beach behind dual-submerged breakwaters. *Ocean Engineering* **45**, 38–55. doi:10.1016/j.oceaneng.2012.01.030.

Ji, C. Y., Chen, X., Cui, J., Yuan, Z. M. & Incecik, A. 2015 Experimental study of a new type of floating breakwater. *Ocean Engineering* **105**, 295–303.

Ji, C. Y., Chen, X., Cui, J., Yuan, Z. M. & Incecik, A. 2016 Experimental study on configuration optimization of floating breakwaters. *Ocean Engineering* **117**, 302–310.

Ji, C. Y., Cheng, Y., Yang, K. & Oleg, G. 2017 Numerical and experimental investigation of hydrodynamic performance of a cylindrical dual pontoon-net floating breakwater. *Coastal Engineering* **129**, 1–16.

Ji, C. Y., Bian, X. Q., Cheng, Y. & Yang, K. 2018 Experimental study of hydrodynamic performance for double-row rectangular floating breakwaters with porous plates. *Ship and Offshore Structure*. https://doi.org/10.1080/17445302.2018.1558521.

Karami, H. & Ghazvinian, H. 2022 A practical and economic assessment regarding the effect of various physical covers on reducing evaporation from water reservoirs in arid and semi-Arid regions (Experimental study). *Iranian Journal of Soil and Water Research ISNN* **53** (6), 1297–1313.

Karami, H., Ghazvinian, H. & Dadrasajirlou, Y. 2023 Application of statistical and geostatistical approaches in temporal and spatial estimations of rainfall. *Journal of Water and Climate Change* **14** (5), 1696–1722.

Kramer, M., Zanuttigh, B., van der Meer, J. W., Vidal, C. & Gironella, F. X. 2005 Laboratory experiments on low-crested breakwaters. *Coastal Engineering* **52** (10–11), 867–885. doi:10.1016/j.coastaleng.2005.09.002.

Laju, K., Sundar, V. & Sundaravadivelu, R. 2011 Hydrodynamic characteristics of pile supported skirt breakwater models. *Applied Ocean Research* **33** (1), 12–22. doi:10.1016/j.apor.2010.12.004.

Liu, Y. & Li, H. 2013 Wave reflection and transmission by porous breakwaters: A new analytical solution. *Coastal Engineering.* **78**, 46–52.

Liu, Z. & Wang, Y. 2020 Numerical studies of submerged moored box-type floating breakwaters with different shapes of cross-sections using SPH. *Coastal Engineering* **158**, 103687.
Melito, I. & Melby, J. A. 2002 Wave runup, transmission, and reflection for structures armored with CORE-LOC. *Coastal Engineering* **45** (1), 33–52. doi:10.1016/S0378-3839(01)00044-8.
Mirzaii, I. & Passandideh-Fard, M. 2012 Modeling free surface flows in presence of an arbitrary moving object. *International Journal of Multiphase Flow* **39**, 216–226.
Nichols, B. D., Hirt, C. W. & Hotchkiss, R. S. 1980 *SOLA-VOF: A Solution Algorithm for Transient Fluid Flow with Multiple Free Boundaries, Tech. Rep. LA-8355*. Los Alamos Scientific Laboratory, Los Alamos, NM, USA.
Peng, Z., Zou, Q., Reeve, D. E. & Wang, P. X. 2009 Parameterization and transformation of wave asymmetries over a low-crested breakwater. *Coastal Engineering* **56** (11–12), 1123–1132. doi:10.1016/ j. coastaleng.2009.08.005.
Rafic, Y. & Pascal, L. 2009 Design optimization of floating breakwaters with an interdisciplinary fluid-solid structural problem. *Canadian Journal of Civil Engineering* **36**, 1732–1743.
Saghi, H. 2018 Entropy generation minimization for the sloshing phenomenon in half-full elliptical storage tanks. *Physica A: Statistical Mechanics and its Applications* **491** (2018), 972–983.
Saghi, H. & Lakzian, E. 2017 Optimization of the rectangular storage tanks for the sloshing phenomena based on the entropy generation minimization. *Energy.* **128**, 564–574.
Saghi, H. & Lakzian, E. 2019 Effects of using obstacles on the Dam break flow based on entropy generation analysis. *The European Physical Journal Plus.* **134** (5). doi:10.1140/epjp/i2019-12592-3.
Saghi, H., Ketabdari, M. J. & Booshi, S. 2012 Generation of linear and nonlinear waves in numerical wave tank using clustering technique-volume of fluid method. *Applied Mathematics and Mechanics (English Edition)* **33**, 1179–1190.
Saghi, H., Mikkola, T. & Hirdaris, S. 2021 A machine learning method for the evaluation of hydrodynamic performance of floating breakwaters in waves. *Ships and Offshore Structures* doi:10.1080/17445302.2021.1927358.
Samii, A., Karami, H., Ghazvinian, H., Safari, A. & Dadrasajirlou, Y. 2023 Comparison of DEEP-LSTM and MLP models in estimation of evaporation pan for arid regions. *Journal of Soft Computing in Civil Engineering* **7** (2), 155–175.
Saremi, S., Mirjalili, S. & Lewis, A. 2017 Grasshopper optimisation algorithm: Theory and application. *Advances in Engineering Software* **105**, 30–47.
Shen, Y. M., Ng, C. O. & Zheng, Y. H. 2004 Simulation of wave propagation over a submerged bar using the VOF method with a two-equation turbulence modeling. *Ocean Engineering.* **31**, 87–95.
Srivastava, S. & Sahana, S. K. 2019 Application of bat algorithm for transport network design problem. *Applied Computational Intelligence and Soft Computing* **2019** (1), 9864090.
Suykens, J. A. 2001 Nonlinear modelling and support vector machines. In: *Instrumentation and Measurement Technology Conference, 2001, IMTC 2001, 1 Proceedings of the 18th IEEE*, pp. 287–294.
Taylor, K. E. 2001 Summarizing multiple aspects of model performance in a single diagram. *Journal of Geophysical Research: Atmospheres* **106** (D7), 7183–7192.
Van der Meer, J. W. & Daemen, I. F. R. 1994 Stability and wave transmission at low crested rubble mound structures. *Journal of Waterway, Port Coastal and Ocean Engineering* **120** (1), 1–9. doi:10.1061/(ASCE)0733-950X (1994)120:1(1).
Yang, X. S. 2009 Firefly algorithms for multimodal optimization. *Stochastic Algorithms: Foundations and Applications.* **5792**, 169–178.
Yang, X. S. & Deb, S. C. 2009 Cuckoo search via Lévy flights. In: *IEEE World Congress on InNature and Biologically Inspired Computing*, pp. 210–214.
Yang, X. S. & Deb, S. 2014 Cuckoo search: Recent advances and applications. *Neural Computing and Applications* **24** (1), 169–174.
Yang, X. S. & He, X. 2013 Firefly algorithm: Recent advances and applications. *International Journal of Swarm Intelligence* **1** (1), 36–50.
Youngs, D. L. 1982 Time-dependent multi-material flow with large fluid distortion. *Numerical Methods for Fluid Dynamics*, 273–285.
Zhang, S. & Li, X. 2014 Design formulas of transmission coefficients for permeable breakwaters. *Water Science and Engineering* **7**, 457–467.

First received 6 December 2023; accepted in revised form 15 July 2024. Available online 7 August 2024